Interphase Mass Transfer of the High Velocity Bubbling Fluidization Regime

Jean Saayman[1*] and Willie Nicol[1]

[1] *Department of Chemical Engineering*
University of Pretoria - Main Campus
Corner Lynwood Rd & Roper St
Hatfield
Pretoria
0002
South Africa

* *Corresponding author:* **Jean Saayman**

Email:	jeansaayman@gmail.com
Phone:	+2784 513 4079
Postal Address:	*Dr. Jean Saayman*
	Department of Chemical Engineering
	University of Pretoria - Main Campus
	Corner Lynwood Rd & Roper St
	Hatfield
	0002
	South Africa

Abstract

Gas-solid fluidization experiments were performed in two separate experimental setups with similar dimensions. Fast X-Ray Tomography (XRT) was used in setup 1, while ozone decomposition experiments were performed in setup 2. Packing and operation characteristics for the two setups were close to identical. The hydrodynamic measurements from the XRT acquisitions were used to evaluate the interphase mass transfer characteristics obtained from the ozone decomposition results. Superficial velocities (U_0) spanning the bubbling up to the onset of the turbulent regime (U_c) were employed. Traditional specific interphase mass transfer (k_{be}) correlations are based on incipiently fluidized beds; however, results suggested that a distinction should be made between the low-interaction bubbling regime and the high-interaction bubbling regime. A change in mass transfer behaviour occurred around a U_0/U_c value of 0.25. An empirical correlation for k_{be} of the high-interaction bubbling regime is

proposed. The correlation gave the best fit for the entire velocity range with an average error of 8%, although it is not recommended for U_0/U_c<0.17. It was observed that the classical approach of penetration theory for interphase mass transfer, performed exceptionally well at low velocities (U_0/U_c<0.34).

KEYWORDS: Fluidization hydrodynamics; Ozone decomposition reaction; X-ray tomography; Interphase mass transfer.

1. Introduction

Catalytic Gas-Solid Fluidized Bed Reactors (FBRs) have been studied and used for over six decades. From novel laboratory demonstrations [1] to performing nanoparticle coatings [2], to being at the heart of large petrochemical companies [3,4], these reactors have many uses. From an engineering point of view, advantages include: efficient solids mixing, good gas-solid contacting and low pressure drop. A wealth of understanding of the hydrodynamics of FBRs and their effects on reactor performance has been gained, although there are numerous areas where fundamental understanding is lacking; examples include modelling, the applicability of two phase theory and the accuracy of interphase mass transfer correlation for different regimes. Many studies mainly focus on either a specific hydrodynamic parameter or the reactor performance. Few studies have followed an integrated approach, which creates difficulties in modelling an FBR. Depending on the operating velocity (U_0) several regimes exist in FBRs, most commonly used being the bubbling, turbulent or fast fluidization regimes. Each regime is characterized by its own hydrodynamic behaviours. The bubbling and fast fluidization regimes have enjoyed much academic attention due to the distinctness of the bubbles and the core annulus, respectively. The turbulent regime has better gas-solids contacting than the bubbling regime without the high solids circulation of the fast fluidization regime. These reasons make the turbulent regime a popular choice for industry. Commercial examples of turbulent reactors include FCC regenerators, zinc sulphide roasters and Mobil MTG, acrylonitrile, maleic anhydride, phthalic anhydride and ethylene dichloride reactors. Despite the turbulent regime being popular in industry, it has not received as much attention as the bubbling or fast fluidization regimes. [5]

Based on observations of incipiently fluidized bubbling beds, the need for hydrodynamic descriptions of two-phase behaviour arose. The earliest well-known published works on the

matter were those of Rowe and Partridge [6,7] and Davidson and Harrison [8–10]. The concept was developed further and gas exchange between the phases was explored [11–16]. Ultimately, leaders in the field such as Kunii, Levenspiel and Grace proposed reactor models based on the theory [17–22]. Generally, these reactor models and the two-phase theory best describe the hydrodynamic behaviour of bubbling fluidized beds [23–26]. The theory entails that most of the gas reagents are contained in a lean, solids/catalyst-deprived phase that bubbles though a dense, solids-rich (emulsion) phase. This closely resembles the physical phenomena in the FBR. Since most of the gas throughput is present in the lean phase, the movement of gas into and out of the emulsion phase often dictates the performance of an FBR. Therefore the description of the interphase mass transfer becomes one of the crucial modelling variables. Most correlations for this transfer are derived on the basis of low-velocity/interaction bubbling regime behaviour with small U_0/U_c values of 0.02, where U_c is the onset velocity of the turbulent regime. In this low U_0/U_c regime the bubbles have near-ideal geometries and low interactions with each other. Despite the success of these models at lower velocities, the transfer correlations are not suited for higher velocity operations [25,27–29].

Few attempts have been made to adapt interphase mass transfer correlations for the higher velocity bubbling regime or turbulent regime [30]. Studies have been conducted where the performance of existing mass transfer correlation have been investigated. Using inert tracer-gas experiments Wu and Agarwal looked at the effects of temperature in a fluidized bed [27]. This study was done in a 127 mm ID column with a bed of particles which was incipiently fluidized using pure nitrogen gas, while single argon gas bubbles were injected near the distributor at the bottom of the bed. These Argon containing bubbles travelled upwards to the top of the bed where a tube extracted a sample of the bubble's gas as the bubble passed the tube. Experiments were conducted using particles from 264 μm to 463 μm and at temperatures of 298 K, 423 K, 573 K and 773 K. The Sit and Grace [16] and Davidson and Harrison [9] correlations were tested. Wu and Agarwal [27] found that the Sit and Grace correlation performed better, but in some cases was not ideal. They incorporated a correction factor for the convection term.

When it comes to reactions in a freely bubbling bed, concentration gradients steepen due to reaction in the cloud phase and bubble interaction starts playing a big role. Thompson et al. [25] used the data of Sun [28] in a new transitional two-phase model. They had to incorporate a correction factor to the Sit and Grace [16] correlation to fit the data. This might be due to the effect of the probabilistic transition factor present in the model. Campos et al. [29]

performed reactor performance experiments in a coke combustor at 1 223 K and inferred mass transfer using two-phase theory. The researchers tested the overall mass transfer correlation of Kunii and Levenspiel and found that the correlations far over-predicted mass transfer. Although, Kunii and Levenspiel warn that the overall mass transfer correlation, which is based on a two-step mass transfer process and a three-phase model, cannot be reduced to a two-phase model for reacting systems [31]. The book of Kunii and Levenspiel [31] is also recommended for a general overview of the field of fluidization.

An integrated approach combining hydrodynamics and reactor performance is followed in this study with the focus on the upper end of the bubbling regime and the start of the turbulent regime. The aim is to investigate which theories in the literature are applicable and which do not hold in a more "violently" bubbling bed. This is achieved by performing in-depth hydrodynamic investigations into a reactive fluidized bed. All experiments are executed at atmospheric conditions using sand particles and two setups. A reaction setup and an advanced X-Ray Tomography (XRT) setup both equipped with pressure sensors are used. The same particles and column diameter are implemented in both setups. Detailed results of the XRT-obtained hydrodynamic insights are reported in previously published work and will be incorporated in this work [32,33]. All reaction experiments are conducted in a 14 cm column using the ozone decomposition reaction and spanning the bubbling to turbulent onset regimes ($0.09 < U_0/U_c < 1.11$). Reactor performance is quantified using a basic two-phase model to obtain the apparent overall mass transfer.

2. Experimental

The XRT setup was a 1.4 m high acrylic column, 140 mm in diameter. Three X-ray sources were positioned around the column as well as three detector arrays opposite each source. Each detector array contained two rows of 32 detectors. This configuration allowed for advanced cross sectional hydrodynamics measurements and tomographic reconstructions. Details on this setup, the measurement techniques and results are previously published [32,33]. The reaction setup was a 140 mm (ID) acrylic column with a height of 5.5 m, which was used to conduct reaction performance experiments. The ozone decomposition reaction was implemented to gauge the FBR's reactor performance. This reaction is popular in FBR experiments due to its first order nature and the small quantities required for analysis resulting in negligible volume change and heat generation [1,15,28,34]. A third packed bed test reactor, with ideal plug flow behaviour and no hydrodynamic influences, was used solely

to determine the first order rate constant of the catalyst being utilized in the FBR reaction setup. Two cyclones in series were used to return entrained solids to the bed. The primary cyclone was a volute cyclone in order to handle high solids loading and the secondary cyclone was a tangential cyclone. An exhaust system with a solids filter bag container was installed after the cyclones to remove any remaining solids safely and to dispose of ozone-containing air via a stack. The filter bags were weighed before and after experiments and solids losses were found to be negligible. Absolute pressure transmitters were installed at the distributor, 0.2 m from the distributor and 0.4 m from the distributor. Figure 1 schematically shows the equipment setup. The fluidizing air supply was dosed with ozone and inlet ozone samples were continuously drawn from the centre of the plenum chamber, 50 mm below the distributor. Outlet samples were taken at a height of 4.2 m above the distributor. Catalyst activity was determined in a 16.4 mm (ID) test reactor with plug flow behaviour. To ensure the catalyst samples were not exposed to an atmosphere other than that inside the FBR the test reactor could be loaded using the fluid nature of a fluidized bed and tapping catalyst directly from the FBR. Both the FBR and the test reactor were supplied with the same ozone-dosed air. The test reactor was designed to detach safely from the FBR, to weigh and empty the loaded catalyst sample. The setup and equipment is discussed in more detail elsewhere [35].

To activate sand for ozone decomposition, the particles require treatment. Iron oxide is consequently impregnated onto the particles. The method of Fan et al. was adopted [34,36]. The particles are mixed into a stirring solution of 10 wt.% ferric nitrate. After 1 h the stirrer is switched off and the solids are allowed to settle out for 15 min. Excess solution is decanted and the sludge placed in an oven for 12 h, resulting in dried solid chunks. These chunks are ground and sieved to the correct size fraction. Lastly, the batch is placed in a furnace at 475 °C to calcinate the impregnated ferric nitrate to ferric oxide. The calcination reaction is as follows:

$$Fe(NO_3)_3.nH_2O \xrightarrow{\geq 370^{\circ}C} \frac{1}{2}Fe_2O_3 + 3NO_2 + \frac{3}{4}O_2 + nH_2O \quad (1)$$

As shown, NO_2 gas is released during the calcination process. When no NO_2 is detected, the reaction has reached completion; this takes approximately 2.5 h.

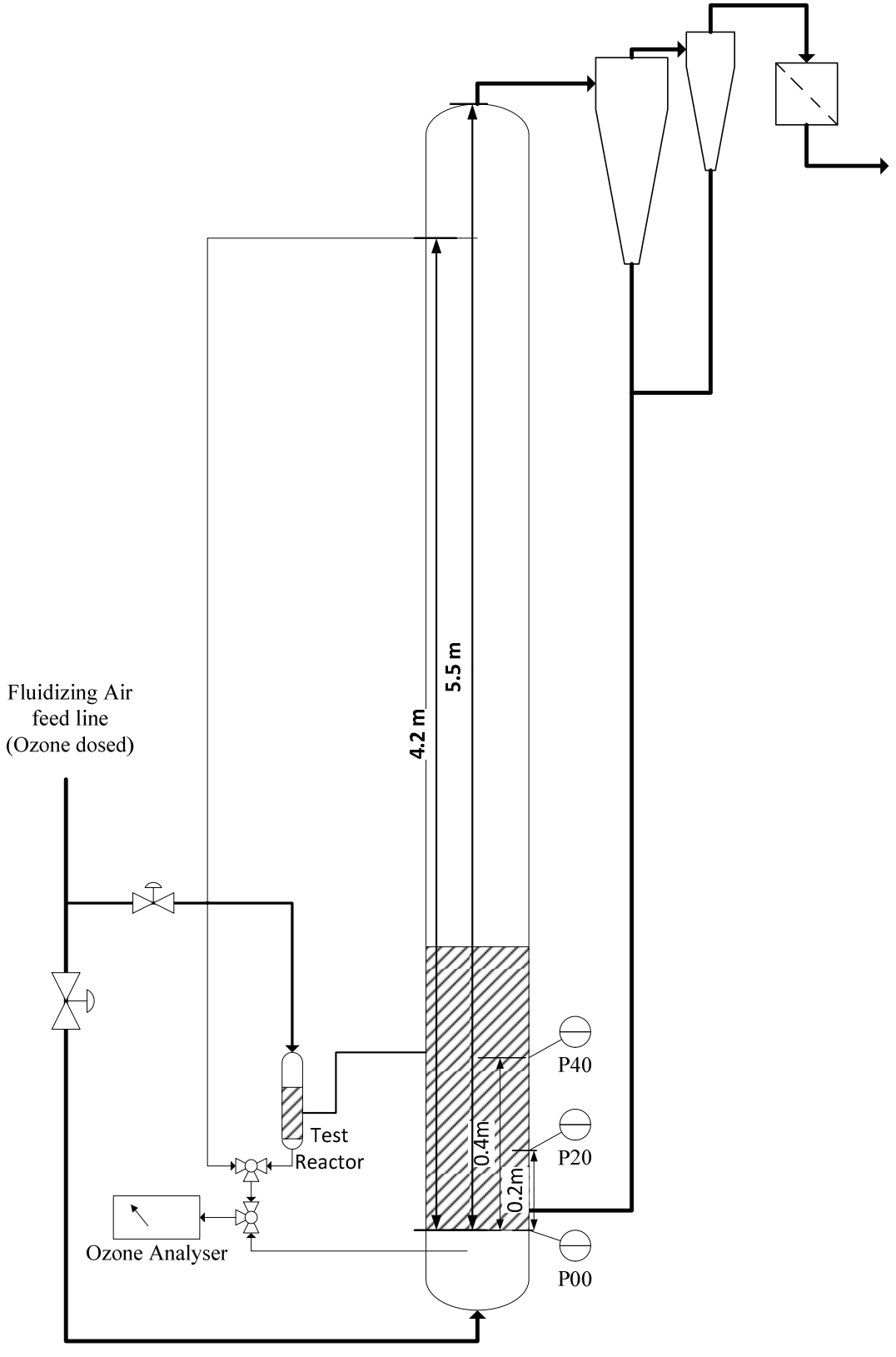

Figure 1: Reactor experimental setup and schematic drawing.

2.1 Method

Before experiments were started, first-order behaviour was confirmed using the small test reactor. Catalyst was loaded into the test reactor and the conversion determined at different flow rates and inlet ozone concentrations. These measurements were made in a relatively short period. A first-order reaction rate Plug Flow Reactor (PFR) model predicted the conversion results accurately, as shown in Figure 2. The first order rate constant (k_R) was 15 s^{-1} during the verification experiment.

During experiments the test reactor was used to check the activity of the catalyst inside the FBR. A sample of the bed was taken and the catalytic activity was determined for each measurement of the FBR's conversion. The FBR and test reactor were run in parallel. Care was taken to sample catalyst out of the FBR into the test reactor without exposing the sample to a different atmosphere. Both reactors were supplied with the same feed gas and advantage was taken of the liquid nature of fluidization to "tap" catalyst directly into the test reactor. In this way variations in the bed activity are accounted for, instead of trying to stabilize the catalyst activity. During operations the test reactor was run at a single velocity since first-order behaviour was known. After each FBR conversion reading, a catalyst sample was taken and the activity determined within 5 min. In this manner a pseudo-instantaneous catalyst activity was obtained. The detachable design of the test reactor made catalyst unloading and weighing between measurements possible.

The following procedure was completed to determine the FBR's conversion. The FBR was set to a specific superficial velocity. The outlet gas-sampling probe was operated in reverse to backwash the filter. High-pressure air from the plenum chamber was used. After the filter had been cleaned, the FBR's outlet concentration was measured for 90 s. Sampling was then switched to the plenum chamber to determine the inlet concentration for 90 s. Lastly, a fresh catalyst sample was loaded into the test reactor and the reaction rate constant determined within 5 min. In a single experimental run this procedure was repeated at 11 different superficial velocities. Three experimental runs were conducted with different means of velocity sequences: low to high; high to low and a random selection.

The FBR was loaded with 13.5 kg of activated sand which resulted in a bed height of 520 mm. It was determined that 14 wt.% of catalyst was in the return system. For the range of superficial gas velocities studied, the settled bed height did not change significantly. The amount of catalyst in the return system therefore remained fairly constant. System properties are reported in Table 1.

Table 1: Catalyst and fluidizing medium properties.

	System properties
ρ_p (kg/m^3)	2 450
ρ_b (kg/m^3)	1 450
$\overline{d_p}$ (μm)	101
Geldart	B
U_{mf} (mm/s)	9.1
ε_{mf}	0.41
μ_g (Pa.s)	18 x 10^{-6}
ρ_g (kg/m^3)	1.2
D_m (m^2/s)	20 x 10^{-6}

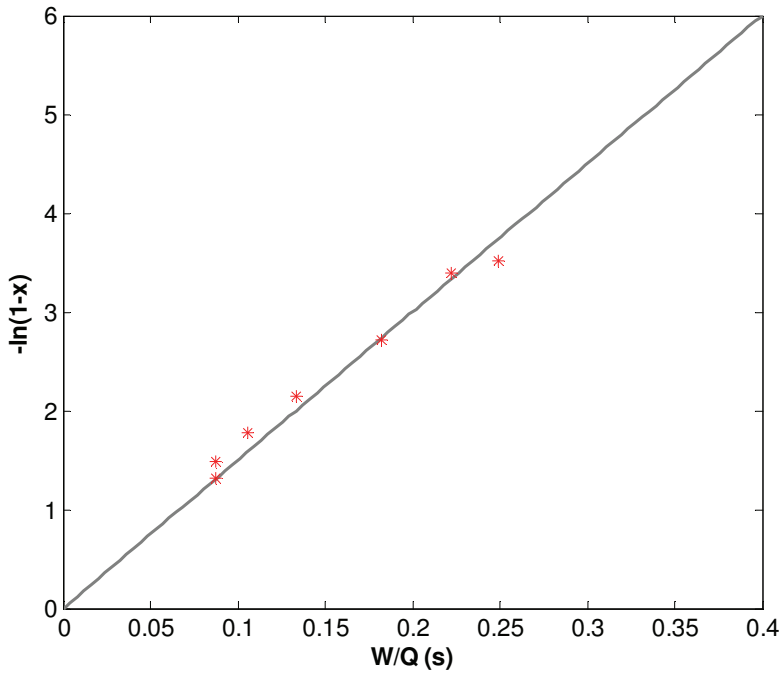

Figure 2: Confirmation of first-order behaviour. The linear line is a first-order PFR model with kR = 15 s-1.

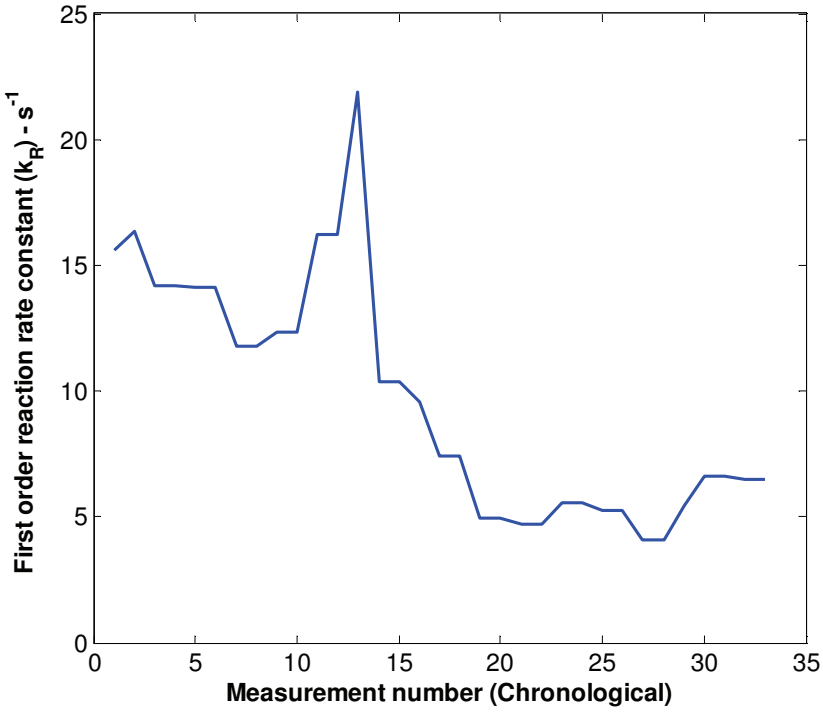

Figure 3: In-situ measurements of ozone decomposition rate constants (kR) performed in the test PFR test reactor.

3. Results and discussion

3.1 Reactor performance

Initial work to quantify reactor performance was done using an FCC catalyst in a pseudo-2D column [37,38]. The Thompson et al. [25] model was used to do a best fit of the reactor performance over the velocity range and ascertain the mass transfer and axial dispersion. As shown by both Brink et al. [37] and Saayman [38], the shape of the fitted curve is dependent on the catalyst activity; therefore, if the activity changes significantly and the reactor is not fully mass transfer controlled, the method fails. Catalyst activity for sand is shown in Figure 3. Large changes and fluctuations in the activity are seen. These are caused by catalyst deactivation and humidity fluctuations respectively [39]. The humidity of the fluidizing air oscillated (1.5 h cycles), creating further activity fluctuations. This behaviour was caused by the compressor's chiller/dehumidifier.

Using FeSi catalyst an alternative method of interpretation was developed where data points could be evaluated individually [35]. The technique entails fitting the basic two-phase model to experimental data using the overall mass transfer coefficient (K0) as fitting parameter. The two-phase model is derived using mass balances for the individual bubble-phase and emulsion-phase [21,31]. These mass balances result in 3 equations:

$$C_i = u_B C_{i,B} + u_E C_{i,E} \tag{2}$$

$$A_{bed} u_B \frac{dC_{i,B}}{dW} = -K_O (C_{i,B} - C_{i,E}) \tag{3}$$

$$A_{bed} u_E \frac{dC_{i,E}}{dW} = -R_i (C_E) + K_O (C_{i,B} - C_{i,E}) \tag{4}$$

The advantage of this approach is that only one parameter is fitted and all complexities of the Thompson et al. [25] model are avoided. It is important to understand when fitting this model to experimental data that K_0 will be an apparent parameter, similar to an apparent reaction rate constant. The value of K_0 will be influenced by hydrodynamic behaviour, which is not considered in the model; hence it is referred to as an "apparent overall mass transfer coefficient". Due to K_0's incorporation of hydrodynamic effects, it serves as a good indicator of the reactor's performance, irrespective of the catalytic activity.

Using the basic two-phase model, reactor conversion and catalyst activity at a superficial velocity, K_0 could be determined. Due to the implicit nature of the model, K_0 was fitted until the model conversion and the actual conversion matched within ±1%. Figure 4 shows K_0, the reactor performance, with the average of the three measurements at a superficial velocity. Reactor performance increased up to a superficial velocity of 0.45 m/s, after which a

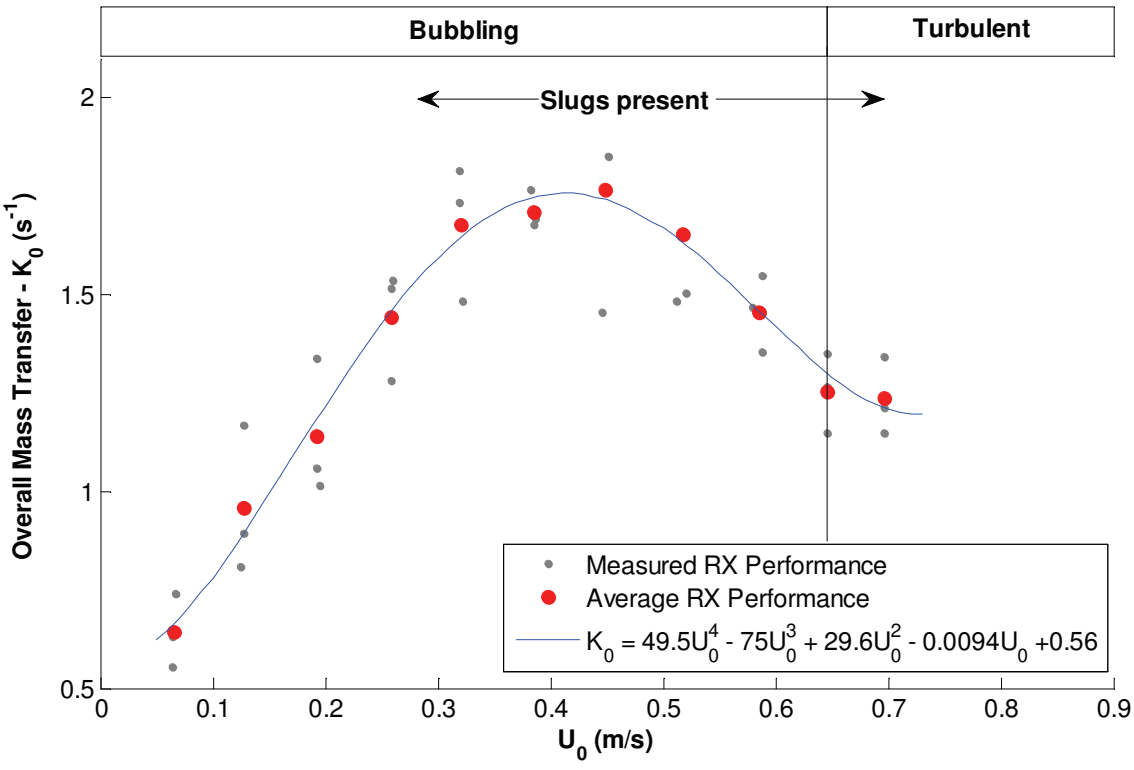

Figure 4: Reactor performance and fitted polynomial for interpolation. Experiments were repeated 3 times (grey) and the averages are shown in red.

decreasing trend was observed. This behaviour cannot be explained directly by the observed slugging, as slugging started at approximately 0.25 m/s and further exploration is required to address the issue (see section 3.2 and 3.3). For integration between the reaction measurements and the XRT measurements, a fit is required. As mentioned the hydrodynamic parameters were measured using an XRT setup with the same sand particles and a 140 mm column. Details on that setup and results of the investigation were already published [32,33]. Each investigation was performed at different superficial velocities and interpolation of reactor performance will be required. A fourth-order polynomial was used, as fourth order accurately preserves the shape. Excessive extrapolation outside the velocity range of 0.06 m/s to 0.705 m/s is not recommended.

3.2 Hydrodynamics

This section compares and confirms the hydrodynamic similarity between the reaction setup and the XRT setup. The transition between the bubbling and turbulent fluidization flow regimes was determined using the standard deviation of pressure fluctuations technique [5]. When using absolute pressure measurements, a clear trend in the standard deviation could not be found. However, the differential pressure measurements between the 20 and 40 cm pressure probes did show a clear trend, as seen in Figure 5. The standard deviation of pressure fluctuations of both the reaction and the XRT column are shown. U_c was the same for both columns at 0.65 m/s. The XRT values are lower since these were determined using an absolute pressure signal and not a differential pressure signal.

The non-intrusive technique of Van der Schaaf et al. [40] was used for monitoring bubble behaviour in the reaction setup. This technique makes use of two pressure probes, one probe at the distributor and the second at a height in the bed where bubble measurement is desired. The Power Spectral Densities (PSDs) of both pressure probe signals are compared and the incoherence of the two signals relative to each other is calculated. The standard deviation of this incoherence (σ_i) is a measure of the average bubble/void height. Van der Schaaf et al. [40] proved that relative bubble sizes and slug lengths can be determined using this technique. The magnitude of the effects that fines have on bubble sizes was observed by Beetstra et al. [41] using σ_i. Figure 6 shows good agreement exists between σ_i, measured in the reaction setup and the average void length, measured in the XRT setup. Both measurements were at 200 mm above the distributor in the respective setups. At 0.25 m/s a

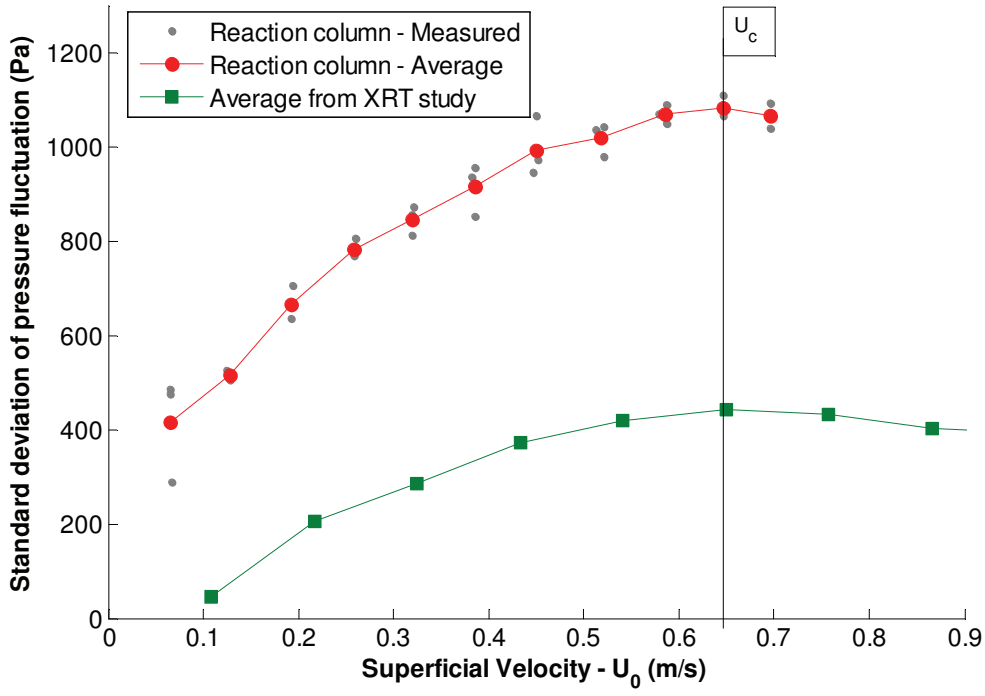

Figure 5: Bubbling to turbulent regime transition confirmed to be at 0.65 m/s for both setups.

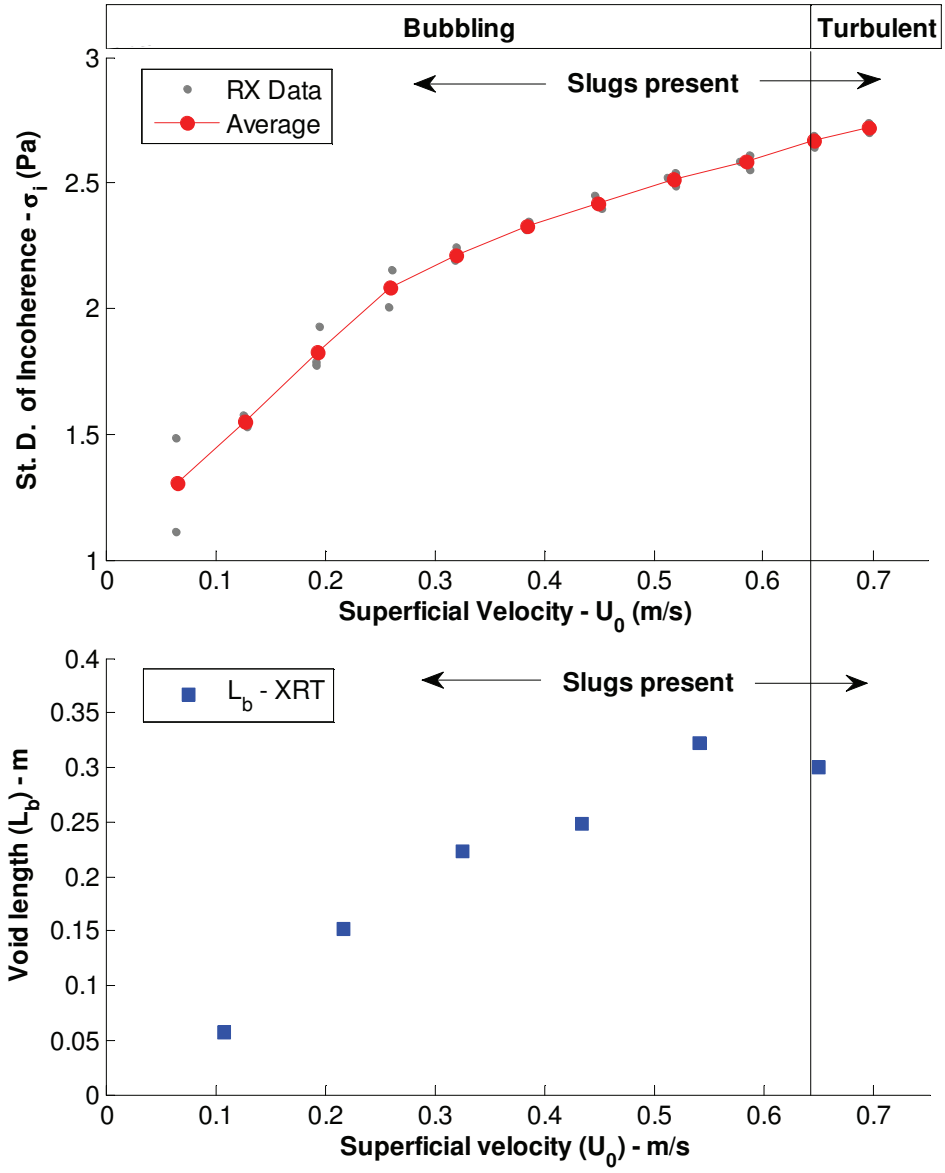

Figure 6: Relative shape agreement between measured standard deviation of incoherence in the reaction setup and the void length, determined using the XRT setup. The standard deviation of incoherence is a measure of the void length.

gradient change occurs due to slug formation. This result is most likely due to the fact that the particle densities and sizes were the same. It can therefore be concluded that the ozone activation treatment of the particles did not influence the hydrodynamic behaviour.

3.3 Link between reactor performance and hydrodynamics

Insight into the reactor performance can be gained using the hydrodynamic information from XRT. The following parameters of individual bubbles were measured using the XRT method:

- Void volumes – V_b
- Void lengths – L_b
- Void rise velocities –U_b
- Cross-sectional solids concentration – Φ_0

Assuming the bubble contains negligible solids, the voids fraction is:

$$\psi_B = \frac{\Phi_{mf} - \Phi_0}{\Phi_{mf}} \tag{5}$$

A cylindrical shape approximates voids more accurately than a spherical shape for this system [32,33]; therefore, the external bubble area per bubble volume can be calculated as follows:

$$d_{b(Cyl)} = \sqrt{\frac{4V_b}{\pi L_b}} \tag{6}$$

$$A_{b(Cyl)} = 2 * \left\{\frac{\pi}{4}\left(d_{b(Cyl)}\right)^2\right\} + \pi L_b d_{b(Cyl)} \tag{7}$$

$$a_I = \frac{A_b}{V_b} \tag{8}$$

Lastly, the terminal bubble rise velocity (U_{br}) can be calculated from:

$$U_{br} = U_b + U_{mf} - U_o \tag{9}$$

The hydrodynamic considerations will be based on parameter averages calculated over the height of the reactor. This is because K_0 is an averaged parameter of the reactor. No single parameters showed a turning behaviour and it is reasonable to assume that a combination of parameters is required to explain the trend. From the literature it is known that rise velocities are linked to specific mass transfer rates. Foka et al. [30] used the superficial velocity of which the rise velocity is a function. U_0 will therefore also be considered alongside the other measured hydrodynamic parameters. Let K_0 be proportional to a power law relationship of the measured variables a_I, ψ_B, Φ_0 and U_0:

$$K_0 \propto \left({a_I}^k {\psi_B}^l {\Phi_0}^m {U_0}^n\right) \quad (10)$$

The Levenberg-Marquardt minimization algorithm (FSOLVE) of Matlab® was used (with k, l, m and n as the numbers to be minimized) in order to find a correlation between K_0 and the parameters a_I, ψ_B, Φ_0 and U_0, the following combination had the best agreement with K_0 – k = 0.936; l = 1.985; m = -2.064; n = -0.992. These numbers are very close to whole numbers and it was found that the whole numbers resulted in an almost exact residual value:

$$K_0 \propto \frac{{a_I}^1 {\psi_B}^2}{{\phi_0}^2 {U_0}^1} \quad (11)$$

Figure 7 shows this combination of parameters with U_0 and the reactor performance with U_0. For both a turn is observed at 0.45 m/s.

3.4 Specific interphase mass transfer

The ideally structured and well-behaved voids of low velocity low-interaction bubbling beds differ considerably from the chaotic structures and behaviours at higher operating velocities. The mass transfer nature of K_0 is investigated by means of the specific interphase mass transfer coefficient (k_{be}). By taking into account the hydrodynamics of the reactor, the K_0 parameter can be converted to the generally used area-specific mass transfer coefficient (k_{be}). K_0 should be multiplied by the solids concentrations and divided by the specific bubble area:

$$k_{be} = \frac{K_O \Phi_0}{\psi_B \, a_i} \quad (12)$$

It needs to be kept in mind that three hydrodynamic elements are assumed to have negligible influence on conversion when using the basic two-phase model:

- Solids content in the total disengagement height (TDH).
- Solids content in the bubbles.
- Gas flow in the emulsion phase is at U_{mf}.

The effects of these elements are incorporated into K_0 and could bias the k_{be} value if they are not negligible. Two of the assumption could be addressed. The validity of the first assumption with regard to the TDH was addressed by measuring the reactor outlet solids concentration/entrainment. Even with an ideal PFR assumption and the freeboard model of Kunii and Levenspiel [42], the contribution to overall conversion was between 5% and 10% of the overall conversion value (relative to overall conversion). This is at the highest flow rate (0.7 m/s), the worst case scenario since the freeboard contribution declines with decreasing

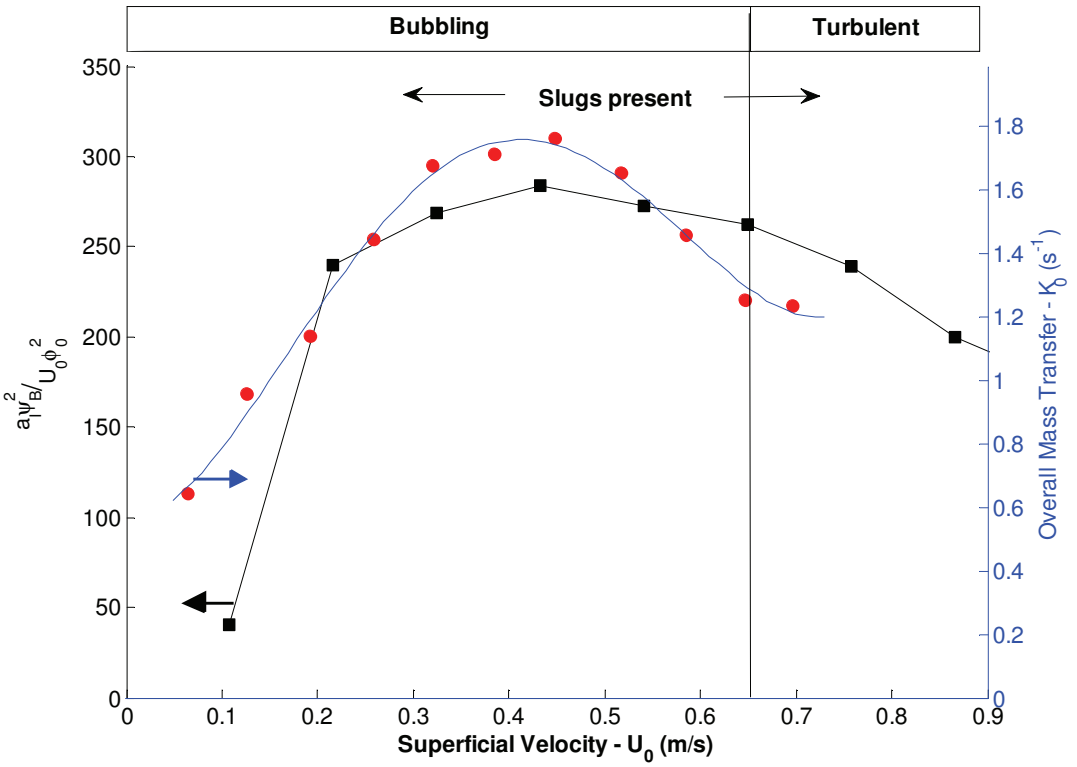

Figure 7: Combination of hydrodynamic parameters having the same trend as the reactor performance parameter K0.

velocity. The TDH assumption was therefore deemed acceptable, especially when considering the bubbling regime to the onset of the turbulent regime. The assumption of negligible bubble solids content can be explored using the observed reactor performance results (Figure 4). Work by Sun and Grace [43] showed that bubble solids content increased with velocity. If the increased solids content was not negligible and significantly influenced K_0, then the decreasing trend beyond 0.45 m/s would not be evident. From the measured parameters the bubble's solids content could not be determined directly. However, the results show indirectly that the possible contribution of solids in the bubble is of a secondary nature and the assumption is acceptable.

There are two types of mass transfer correlation in literature: the first is based on penetration theory and the second on boundary layer equations [13]. Literature correlations are tested to evaluate the applicability over the entire bubbling regime. The absolute value of k_{be} is dependent on the model assumptions, two of which have been deemed acceptable. The following discussion is concerned mainly with the observed trends with superficial velocity.

3.4.1 Penetration theory

In penetration theory k_{be} is generally a linear function of $(U_{br}/d_b)^{1/2}$. d_b represents the void height; it can therefore be replaced by L_b. Considering Sit and Grace:

$$k_{be} = \frac{1}{3}U_{mf} + \left(\frac{4D_m\varepsilon_{mf}U_{br}}{\pi D_b}\right)^{\frac{1}{2}} \quad (13)$$

The absolute correlation does not give a quantitatively good prediction, as seen in Figure 8(A-i). Hence, the constants in the correlation equation are combined:

$$k_{be} = c_{pt} + m_p\left(\frac{U_{br}}{L_b}\right)^{\frac{1}{2}} \quad (14)$$

c_{pt} and m_p represent all the constants. Using experimentally determined k_{be} and the XRT measurements for U_{br} and L_b over the entire velocity range of 0.11 m/s to 0.76 m/s, the best fit values for c_{pt} and m_p were determined:

$$k_{be} = -0.0265 + 0.0245\left(\frac{U_{br}}{L_b}\right)^{\frac{1}{2}} \quad (15)$$

Higher velocity k_{be} values and possible experimental error caused the negative value of c_p. Figure 8(A-i) shows the prediction of this equation using XRT data compared with the measured k_{be} using the reactor performance data. The scatter in correlation is due to the scatter in the experimentally determined values for U_{br} and L_b. The absolute percentage error

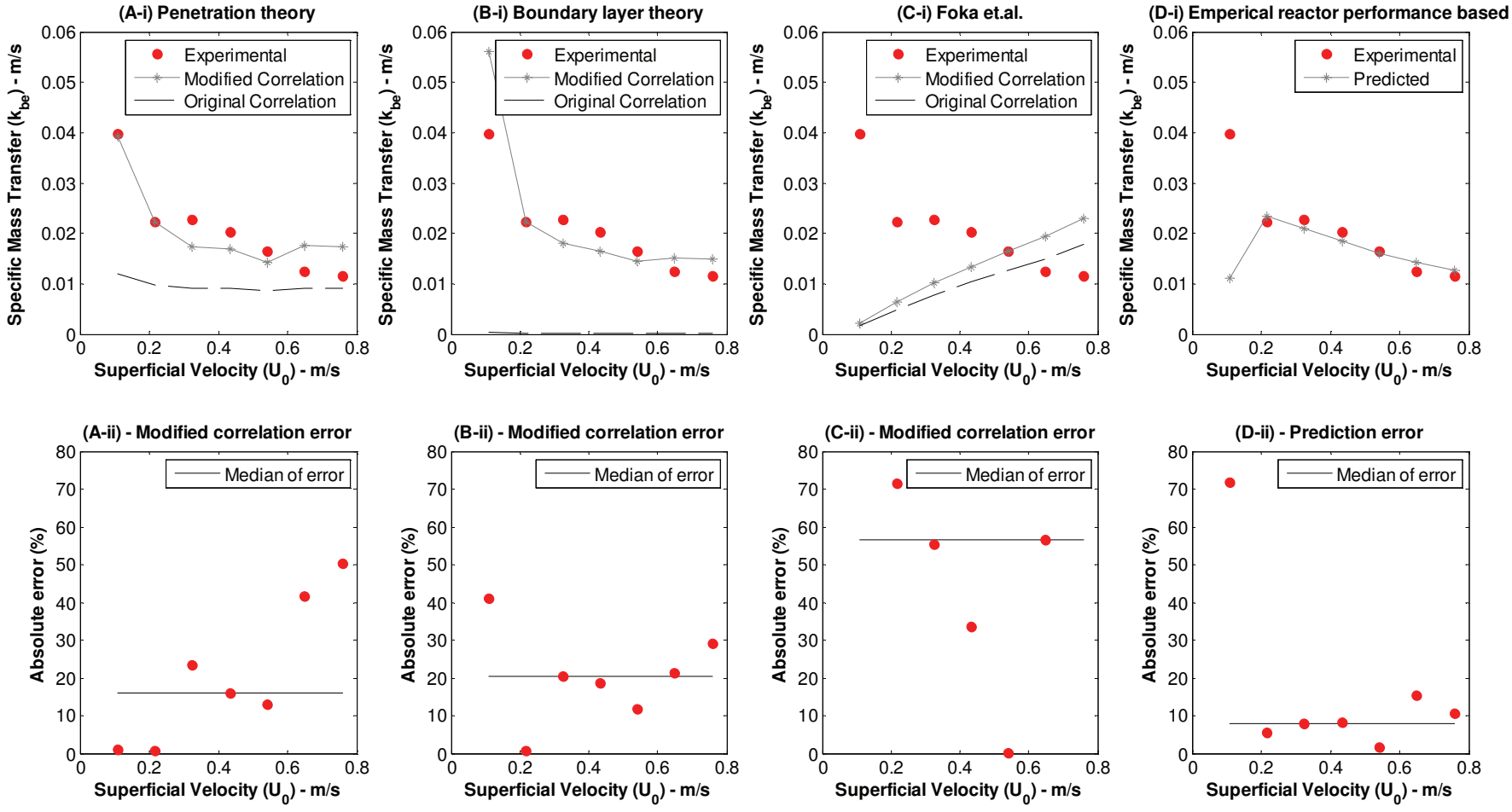

Figure 8: Predicted specific mass transfer compared with the measured specific mass transfer based on several theories and correlations. The error made in the modified correlation prediction is shown.

is shown in Figure 8(A-ii); the line indicates the median error over the entire velocity range. For the entire velocity range the fit is not ideal; however, for the lower velocities (U_0/U_c<0.34) the error is almost zero. This suggests that the mechanism of mass transfer proposed by penetration theory is only valid for low-interaction bubbling reactors.

3.4.2 Boundary layer theory

Two boundary layer correlations are tested, namely Partridge and Rowe [13] and Foka et al. [30]. Foka et al. developed their correlation based on bubbling and turbulent regime data. The correlation by Partridge and Rowe is considered first:

$$\frac{k_{be}a_I\psi_B D_b}{\varepsilon_0 D_m} = 2 + 0.69\left(\frac{\mu_g}{D_m\rho_g}\right)^{1/3}\left(\frac{\rho_g U_{br} D_b}{\mu_g}\right)^{1/2} \quad (16)$$

This correlation performs exceptionally poorly as seen in Figure 8(B-i). From general observations in the literature it is found that authors prefer penetration theory correlations. Following the same argument as above, the constants are combined and a linear equation is obtained:

$$\frac{k_{be}a_I\psi_B L_b}{1-\Phi_0} = c_B + m_B(U_{br}L_b)^{\frac{1}{2}} \quad (17)$$

c_B and m_B are the combinations of all the constants. Using experimentally determined k_{be} and the XRT measurements for U_{br} and L_b over the entire velocity range of 0.11 m/s to 0.76 m/s, the best fit values for c_B and m_B were determined:

$$\frac{k_{be}a_I\psi_B L_b}{1-\Phi_0} = 0.3179 + 0.0366(U_{br}L_b)^{\frac{1}{2}} \quad (18)$$

Figure 8(B-i) and (B-ii) shows the results. Relative to penetration theory, the predicted trend agreement is worse.

The correlation by Foka et al. has a direct proportionality and does not perform well:

$$k_{be}a_I = 1.631Sc^{0.37}U_0 \quad (19)$$

The process of linearization was repeated, except that a linear equation was used which goes through the origin:

$$k_{be} = 1.8997\left(\frac{U_0}{a_I}\right) \quad (20)$$

Figure 8(C-i) shows that the original correlation and the modified correlation do not differ significantly. This is due to fewer degrees of freedom in the number of fitting parameters. Although the correlation was designed to include the entire bubbling and turbulent regime,

the errors are extremely large as shown in Figure 8(C-ii). Bi et al. mentioned that this correlation had not been extensively validated and should be used with caution [5].

3.4.3 Empirical correlation

Based on observations in Figure 7, it is proposed to correlate k_{be} and $\psi_B/(\Phi_0 U_0)$. This parameter is referred to as β:

$$K_0 \propto \frac{{a_I}^1 {\psi_B}^2}{{\phi_0}^2 {U_0}^1} \tag{21}$$

$$\frac{K_0(\phi_0)}{(a_I \psi_B)} \propto \frac{\psi_B}{\phi_0 U_0} \tag{22}$$

$$k_{be} \propto \frac{\psi_B}{\phi_0 U_0} = \beta \tag{23}$$

Performing a linear fit through the origin gives:

$$k_{be} = 0.00568\beta \tag{24}$$

Figure 8(D-i) shows this equation's prediction compared with the measured values and Figure 8 (D-ii) shows the error. At 8% the lowest median of errors over the velocity range is obtained. This combination of hydrodynamic parameters fails to predict at the lowest velocity were ideal bubbling occurs. For the rest of the range (U_0/U_c>0.17) good correlation is observed. The ideally structured and well-behaved voids of low-interaction bubbling beds differ considerably from the chaotic structures and behaviours at higher operating velocities, a single mass transfer correlation suitable for all velocity could therefore not be found. A change in mass transfer behaviour occurs around U_0/U_c = 0.25.

4. Conclusions

A fast X-Ray Tomography (XRT) setup and a reaction setup with close to identical column sizes and packing were used in this investigation. Reactor performance was quantified using a basic two-phase model and an apparent overall mass transfer parameter (K_0). This revised method of analysis and quantification eliminated the need to stabilize the activity of the ozone decomposition catalyst. As superficial velocity increased, K_0 (the reactor performance) increased up to U_0 = 0.45 m/s, after which a decreasing trend was observed. The performance continued to decrease, reaching a plateau with superficial velocity at the bubbling-turbulent regime transition. The hydrodynamic measurements from XRT were used

to evaluate the mass transfer characteristics of K_0. The observed trend could be correlated using the following combination of hydrodynamic parameters:

$$K_0 \propto \frac{{a_I}^1 {\psi_B}^2}{{\phi_0}^2 {U_0}^1} \quad (11)$$

Specific interphase mass transfer (k_{be}) was investigated and it was found there is a distinct difference between low-interaction bubbling regime behaviour and high-interaction bubbling regime behaviour. Using the relationship between K_0 and k_{be}, the above equation was rewritten and an empirical correlation is suggested for k_{be}:

$$k_{be} \propto \frac{\psi_B}{\phi_0 U_0} = \beta \quad (23)$$

β gave the best fit for the entire velocity range with an average error of 8%, although it is not recommended for $U_0/U_c<0.17$. From a comparison of the classical approaches of penetration theory and boundary layer theory it was found that penetration theory performed better at low velocities ($U_0/U_c<0.34$). The boundary between the low-interaction and high-interaction bubbling regimes occurs around a U_0/U_c of 0.25 for this system.

Nomenclature

$A_{b(Cyl)}$	External surface area of cylindrical bubble	[m^2]
A_{bed}	Cross sectional area of the reactor	[m^2]
a_I	Inter-phase transfer surface	[m^{-1}]
$C_{i,B}$	Concentration in bubble	[mol/m^3]
$C_{i,E}$	Concentration in emulsion	[mol/m^3]
C_i	Gas concentration of species I	[$kmol/m^3$]
D_b	Spherical-Volume equivalent bubble diameter	[m]
D_m	Gas diffusion coefficient	[m^2/s]
$d_{b(Cyl)}$	Base diameter of cylindrical bubble	[m]
d_p	Sauter mean particle diameter	[m]
K_0	Overall interphase mass transfer (catalyst volume based)	[s^{-1}]
L_b	Length/height of voids	[m]
k_{be}	Specific interphase mass transfer (bubble to emultion)	[m/s]
k_R	Reaction rate constant (catalyst volume based)	[s^{-1}]
Q	Volumetric flow rate in test reactor	[m^3/s]
R_i	Reaction rate as a function of concentration	[s^{-1}]

Sc	Schmidt number ($\mu/(\rho_g.D_m)$)	[-]
U_b	Average bubble velocity, relative to distributor	[m/s]
u_B	Bubble phase reactor model gas velocity	[m/s]
U_{br}	Terminal rise velocity of a single bubble	[m/s]
U_c	Onset of turbulent regime velocity	[m/s]
u_E	Emulsion phase reactor model gas velocity	[m/s]
U_{mf}	Minimum fluidization velocity	[m/s]
U_0	Operating velocity	[m/s]
V_b	Volume of bubble/void	[m^3]
W	Solids volume of catalyst	[m^3]
X	Conversion	[-]

Greek letters

β	Empirical mass transfer parameter ($\psi_B/(\Phi_0 U_0)$)	[s/m]
ε_{mf}	Gas volume fraction at minimum fluidization	[-]
ρ_b	Bulk density	[kg/m^3]
ρ_p	Particle density	[kg/m^3]
ρ_g	Gas density	[kg/m^3]
μ_g	Gas viscosity	[Pa.s]
σ_i	Standard deviation of incoherence	[Pa]
Φ_0	Solids volume fraction (1-ε)	[-]
Φ_{mf}	Solids fraction of incipiently fluidized bed	[-]
ψ_B	Bubble phase volume fraction	[-]

References

[1] J. Saayman, W. Nicol, Demonstrating the effect of interphase mass transfer in a transparent fluidized bed reactor, Chemical Engineering Education. 45 (2011) 178–183.

[2] J.R. van Ommen, J.M. Valverde, R. Pfeffer, Fluidization of nanopowders: a review., Journal of Nanoparticle Research. 14 (2012) 737.

[3] D.J. Duvenhage, T. Shingles, Synthol reactor technology development, Catalysis Today. 71 (2002) 301–305.

[4] A.P. Steynberg, R.L. Espinoza, B. Jager, A.C. Vosloo, High temperature Fischer–Tropsch synthesis in commercial practice, Applied Catalysis A: General. 186 (1999) 41–54.

[5] H.T. Bi, N. Ellis, I.A. Abba, J.R. Grace, A state-of-the-art review of gas-solid turbulent fluidization, Chemical Engineering Science. 55 (2000) 4789–4825.

[6] P.N. Rowe, B.A. Partridge, E. Lyall, G.M. Ardran, Bubbles in Fluidized Beds, Nature. 195 (1962) 278–279.

[7] P.N. Rowe, B.A. Partrige, Gas flow through bubbles in a fluidized bed - I Flow through an ideal bubble, Chemical Engineering Science. 18 (1963) 511–524.

[8] J.F. Davidson, D. Harrison, The behaviour of a continuously bubbling fluidised bed, Chemical Engineering Science. 21 (1966) 731–738.

[9] J.F. Davidson, D. Harrison, Fluidized Particles, 1st ed., The Syndics of the Cambridge University Press, 1963.

[10] M.J. Lockett, J.F. Davidson, D. Harrison, On the two-phase theory of fluidization, Chemical Engineering Science. 22 (1967) 1059–1066.

[11] G.K. Stephens, R.J. Sinclair, O.E. Potter, Gas Exchange between Bubbles and Dense Phase in a Fluidised Bed, Powder Technology. 1 (1967) 157–166.

[12] K. Godard, J.F. Richardson, Distribution of gas flow in a fluidised bed, Chemical Engineering Science. 23 (1968) 660.

[13] A.A.H. Drinkenburg, K. Rietema, Gas transfer from bubbles in a fluidized bed to the dense phase—I. Theory, Chemical Engineering Science. 27 (1972) 1765–1774.

[14] C. Chavarie, J.R. Grace, Interphase Mass Transfer in a Gas-Fluidized Bed, Chemical Engineering Science. 31 (1975) 741–749.

[15] S.P. Sit, J.R. Grace, Interphase Mass Transfer in an Aggregative Fluidized Bed, Chemical Engineering Science. 33 (1978) 1115–1122.

[16] S.P. Sit, J.R. Grace, Effect of Bubble Interaction on Interphase Mass Transfer in Gas Fluidized Beds, Chemical Engineering Science. 36 (1981) 327–335.

[17] C. Chavarie, J.R. Grace, Performance Analysis of a Fluidized Bed Reactor. II. Observed Reactor Behavior Compared with Simple Two-Phase Models, Industrial & Engineering Chemistry Fundamentals. 14 (1975) 79–86.

[18] C. Chavarie, J.R. Grace, Performance Analysis of a Fluidized Bed Reactor. I. Visible Flow Behavior, Industrial & Engineering Chemistry Fundamentals. 14 (1975) 75–79.

[19] C. Chavarie, J.R. Grace, Performance analysis of a fluidized bed reactor. III. Modification and extension of conventional two-phase models, Industrial & Engineering Chemistry Fundamentals. 14 (1975) 86–91.

[20] J.R. Grace, Generalized Models for Isothermal Fluidized Bed Reactors, in: L.K. Doraiswamy (Ed.), Recent Advances in the Engineering Analysis of Chemically Reacting Systems, New Delhi. Wiley Eastern, 1984: pp. 237–255.

[21] D. Kunii, O. Levenspiel, Fluidized reactor models. 1. For bubbling beds of fine, intermediate, and large particles. 2. For the lean phase: freeboard and fast fluidization, Industrial & Engineering Chemistry Research. 29 (1990) 1226–1234.

[22] D. Kunii, O. Levenspiel, Entrainment of solids from fluidized beds I. Hold-up of solids in the freeboard II. Operation of fast fluidized beds, Powder Technology. 61 (1990) 193–206.

[23] I.A. Abba, J.R. Grace, H.T. Bi, Spanning the Flow Regimes : Generic Fluidized-Bed Reactor Model, AIChE Journal. 49 (2003) 1838–1848.

[24] J. Chaouki, A. Gonzalez, C. Guy, D. Klvana, Two-phase model for a catalytic turbulent fluidized-bed reactor : Application to ethylene synthesis, Chemical Engineering Science. 54 (1999) 2039–2045.

[25] M.L. Thompson, H. Bi, J.R. Grace, A generalized bubbling/turbulent fluidized-bed reactor model, Chemical Engineering Science. 54 (1999) 3–10.

[26] R. Jafari, R. Sotudeh-Gharebagh, N. Mostoufi, Performance of the wide-ranging models for fluidized bed reactors, Advanced Powder Technology. 15 (2004) 533–548.

[27] W. Wu, P.K. Agarwal, The Effect of Bed Temperature on Mass Transfer Fluidized Bed, The Canadian Journal of Chemical Engineering. 81 (2003) 940–948.

[28] G. Sun, J.R. Grace, The Effect of Particle Size Distribution on the Performance of a Catalytic Fluidized Bed Reactor, Chemical Engineering Science. 45 (1990) 2187–2194.

[29] J.B.L.M. Campos, O.D.S. Mota, A.M.F.R. Pinto, Measurement of Mass Transfer between the Bubble and Dense Phases in a Fluidized Bed Combustor, Combustion and Flame. 116 (1998) 105–119.

[30] M. Foka, J. Chaouki, C. Guy, D. Klvana, Gas phase hydrodynamics of a gas-solid turbulent fluidized bed reactor, Chemical Engineering Science. 51 (1996) 713–723.

[31] D. Kunii, O. Levenspiel, Fluidization Engineering, 2nd ed., Butterworth-Heinemann, 1991.

[32] J. Saayman, J.R. Van Ommen, R.F. Mudde, E.C. Wagner, W. Nicol, Fluidization Regimes Characterized Using a Fast X-Ray Tomography Setup, in: F. Berruti (Ed.), The 14th International Conference on Fluidization – From Fundamentals to Products, ECI Symposium Series, 2013.

[33] J. Saayman, W. Nicol, J. R. van Ommen, R.F. Mudde, Fast X-Ray Tomography for the Quantification of the Bubbling-, Turbulent- and Fast Fluidization- Flow Regimes and Void Structures, Chemical Engineering Journal. 234 (2013) 437–447. DOI: http://dx.doi.org/10.1016/j.cej.2013.09.008

[34] C. Fan, X. Bi, W. Lin, W. Song, Mass transfer and reaction performance of the downer and its hydrodynamic explanation, The Canadian Journal of Chemical Engineering. 86 (2008) 436–447.

[35] J. Saayman, N. Ellis, W. Nicol, Fluidization of high-density particles: The influence of fines on reactor performance, Powder Technology. 245 (2013) 48–55.

[36] C. Fan, Y. Zhang, X. Bi, W. Song, W. Lin, L. Luo, Evaluation of downer reactor performance by catalytic ozone decomposition, Chemical Engineering Journal. 140 (2008) 539–554.

[37] H.G. Brink, J. Saayman, W. Nicol, Two Dimensional Fluidised Bed Reactor: Performance of a Novel Multi-Vortex Distributor, Chemical Engineering Journal. 175 (2011) 484–493.

[38] J. Saayman, Bubbling to Turbulent Regime Transition in a 2D Catalytic Fluidized Bed Reactor, University of Pretoria, 2009.

[39] B. Dhandapani, S.T. Oyama, Gas phase ozone decomposition catalysts, Applied Catalysis B: Environmental. 11 (1997) 129–166.

[40] J. Van der Schaaf, J.C. Schouten, F. Johnsson, C.M. Van den Bleek, Non-intrusive determination of bubble and slug length scales in fluidized beds by decomposition of the power spectral density of pressure time series, International Journal of Multiphase Flow. 28 (2002) 865–880.

[41] R. Beetstra, J. Nijenhuis, N. Ellis, J.R. Van Ommen, The Influence of the Particle Size Distribution on Fluidized Bed Hydrodynamics Using High-Throughput Experimentation, AIChE Journal. 55 (2009) 2013–2023.

[42] D. Kunii, O. Levenspiel, The KL reactor model for circulating fluidized beds, Chemical Engineering Science. 55 (2000) 4563–4570.

[43] G. Sun, J.R. Grace, Experimental determination of particle dispersion in voids in a fluidized bed, Powder Technology. 80 (1994) 29–34.